Rapid Detection of Drugs of Abuse in Saliva Using Surface Enhanced Raman Spectroscopy and Microfluidics

Chrysafis Andreou,[†] Mehran R. Hoonejani,[‡] Meysam R. Barmi,[‡] Martin Moskovits,[§] and Carl D. Meinhart[‡,*]

[†]Interdepartmental Program in Biomolecular Science and Engineering, University of California, Santa Barbara, California 93106, United States, [‡]Department of Mechanical Engineering, University of California, Santa Barbara, California 93106, United States, and [§]Department of Chemistry and Biochemistry, University of California, Santa Barbara, California 93106, United States

ABSTRACT We present a microfluidic device that detects trace concentrations of drugs of abuse in saliva within minutes using surface-enhanced Raman spectroscopy (SERS). Its operation is demonstrated using methamphetamine. The detection scheme exploits concentration gradients of chemicals, fostered by the laminar flow in the device, to control the interactions between the analyte, silver nanoparticles (Ag-NPs), and a salt. Also, since all species interact while advecting downstream, the relevant reaction coordinates occur with respect to the position in the channel. The system was designed to allow the analyte first to diffuse into the side stream containing the Ag-NPs, on which it is allowed to adsorb, before salt ions are introduced, causing the Ag-NPs to aggregate, and so creating species with strong SERS signal. The device allows partial separation *via* diffusion of the analyte from the complex mixture. Also, the reproducible salt-induced NP aggregation decouples the aggregation reaction (necessary for strong SERS) from the analyte concentration or charge. This method enables the creation of a region where detection of the analyte of interest *via* SERS is optimal, and dramatically extends the classes of molecules and quality of signals that can be measured using SERS, compared to bulk solution methods. The spatial distribution of the SERS signals was used to map the degree of nanoparticle aggregation and species diffusion in the channel, which, together with numerical simulations, was used to describe the kinetics of the colloid aggregation reaction, and to determine the optimal location in the channel for SERS interrogation.

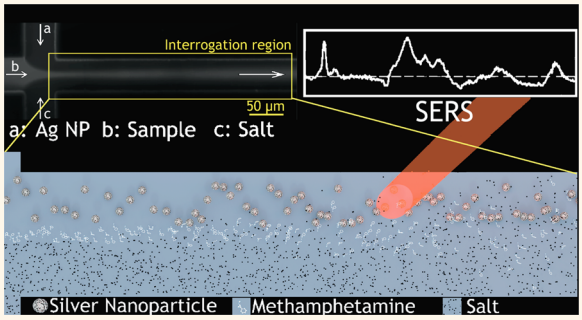

KEYWORDS: surface-enhanced Raman spectroscopy · methamphetamine detection · microfluidics · aggregation kinetics · saliva

A quick, cost-effective method for detection of drugs of abuse in biological or other complex fluids would be of great value in healthcare, law enforcement, and home testing applications. Among such substances, methamphetamine (dextromethamphetamine) is of special importance as its use is growing globally at particularly rapid rates.[1] This is partly due to its low cost and ease of manufacture.

Saliva is the preferred biological fluid for determining the use of drugs taken by mouth. Unlike sampling blood or urine, saliva testing can be carried out noninvasively and under supervision.[2] In addition, for the case of methamphetamine, concentrations in saliva significantly exceed those in blood plasma.[3,4]

Currently, drug testing is usually carried out in laboratories, utilizing methods such as ELISA,[5,6] gas chromatography with mass spectrometry,[7] or HPLC.[8,9] These often require expensive reagents and trained personnel, and may take several hours to complete. On the other hand, commercial drug-screening products for testing at home use the Marquis reagent test, or a similar colorimetric reaction, to determine the presence of a narcotic. Such assays usually test for only a limited number of substances, and require specialized reactants, large sample volumes, and may be misinterpreted by subjective color perception.[10]

Chip-based detection methods can reduce the time of analysis and the cost per sample, by minimizing the quantity of sample and reagents needed, and by allowing multiple tests to be carried out in parallel. Several such methods are presented in reviews by Mogensen *et al.*[11] and Vandaveer *et al.*[12]

* Address correspondence to meinhart@engineering.ucsb.edu.

Received for review May 21, 2013 and accepted July 16, 2013.

Published online July 16, 2013
10.1021/nn402563f

Label-free methods that provide a real-time signal that can be used to identify multiple chemical species coexisting in the same sample are of particular interest. Such a method is surface-enhanced Raman spectroscopy (SERS). A review of SERS-based detection platforms is provided by Lim *et al.*[13]

SERS is a form of vibrational spectroscopy that relies on inelastic light scattering by molecules providing a unique spectroscopic signature potentially identifying the species.[14] The enhancement stems from surface plasmons excited in appropriately nanostructured substrates, that, under favorable conditions, can achieve scattering cross sections upward of 8 orders of magnitude greater than traditional Raman spectroscopy,[15] making detection of even single molecules possible.[16] SERS has previously been used to successfully detect and identify narcotics in trace quantities,[17] as well as for the detection of explosives[18,19] and molecules of biological interest.[20]

SERS detection however is not without problems. For example, certain molecular species that do not have strong affinity for the SERS substrate may be hard to detect. This is particularly true in complex fluids containing multiple species, where moieties with high affinity could bind to the exclusion of other species that may be present. Since methamphetamine has no net charge or appropriate reactive groups, it has relatively low affinity for silver. SERS detection of methamphetamine was shown to be possible, however, *via* chemical modifications that enable it to bind to the substrate.[21] More recently, it was shown that saliva samples can be used to screen for methamphetamine users by SERS by evaporating the sample on an array of nanopillars.[22]

Clearly a quick, SERS-based detection method that allows identification of methamphetamine without requiring chemical modification and specialized reactants would be preferable. Here, we report a microfluidic flow-focusing device that controls and optimizes the interaction of microliter samples of saliva with a SERS substrate based on silver nanoparticles (Ag-NPs) in suspension, enabling the rapid detection of a drug at biologically relevant concentrations. The detection method makes use of the laminar flow profile in the vacuum-driven, hydrodynamic flow-focusing microfluidic device to spatially control the interactions of the nanoparticles, an aggregation-inducing agent, and the sample. Also, being label-free, the method we describe here could also be used for detecting other narcotics, toxins, or disease agents.

In our design, the spatial arrangement and the flow rate of the various streams are tailored for optimal SERS detection. Specifically, the analyte molecules, introduced through the central stream, diffuse laterally into the side streams, and, importantly, into the side stream containing the Ag-NPs, on which the analyte may adsorb. Any larger species that may be present in the sample will diffuse more slowly, so in this way, partial separation of the analyte from the complex fluid is achieved. The Ag-NPs are much more massive than any of the other chemical species involved in the process; hence, they diffuse much more slowly than the molecular species. The salt ions, which play the role of an aggregating agent, diffuse quickly, but they must travel a greater distance before reaching the other side stream, where the Ag-NPs reside, since they must cross the central stream. Hence, significant Ag-NP aggregation only begins after the analyte has had sufficient time to adsorb on the nanoparticles. The strongest SERS signal is observed at a location downstream where abundant aggregates (predominantly dimers and other small order aggregates) abide. This location is determined by collecting Raman signals from various positions in the device, and thus making a spectral mapping of the channel. A schematic of the device, the characteristic diffusion profile of the sample, and the pertinent species interactions are shown in panels A, B, and C, respectively, of Figure 1.

The signal amplification that enables SERS depends critically on the state of aggregation of the nanoparticles.[23] According to the DLVO theory,[24] colloidal particles in suspension remain stable on account of electrostatic repulsion resulting from their surface charge. Aggregation can be induced by processes that reduce the surface charge, for example, by the displacement of surface ions by adsorbates[25] and by pH changes,[26] as well as by ionic screening,[27] and depletion forces.[28]

For the purposes of SERS-based detection, adsorbate-induced aggregation is ideal. But for low-concentration detection, this can be used only when the target analyte has a strong affinity for the colloid. When that is the case, analyte molecules adsorb on the NPs, according to an appropriate adsorption isotherm,[29] displacing the charged species on the surface thereby inducing aggregation. SERS-based detection *via* this mechanism has been successfully demonstrated by Piorek *et al.*[18,19]

Methamphetamine, however, does not have strong affinity for silver and therefore does not promote aggregation reliably. Also, in a complex fluid, a poor adsorber runs the risk of being outcompeted for available adsorption sites on the silver surface by other species. Moreover, different concentrations of adsorbate would cause aggregation at different rates, with the lowest concentration samples requiring long aggregation times to produce useful spectra. We have consequently opted to use salt-induced aggregation, so as to create a reproducible state of nanoparticle aggregation practically independent of the analyte concentration. In the current experiments, lithium chloride was used, inducing aggregation of citrate-capped Ag-NPs predominantly by ionic screening, although chloride ions are known to adsorb on the Ag-NP forming a silver chloride layer.

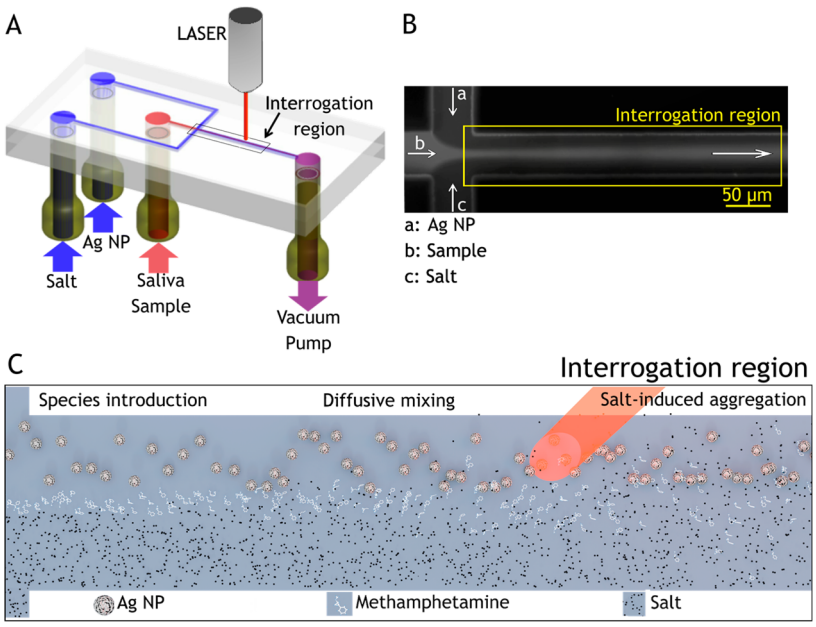

Figure 1. Flow-focusing microfluidic device used for controlled Ag-NP aggregation. (A) Ag-NP suspension, a saliva sample, and salt solution are loaded in the device and driven through it by a vacuum pump. (B) At the flow-focusing junction, the sample stream is enveloped by the side-streams and diffusion drives lateral mass transport between the laminar flows, here visualized with a fluorescent dye. (C) Schematic of the reaction: Ag NP, analyte, and salt solution are introduced to the channel from the left and flow toward the right. Analyte molecules resident in the focused stream diffuse laterally into the side flows. Salt ions also diffuse into the colloid stream inducing controlled nanoparticle aggregation, creating SERS-active clusters that convect downstream. Interrogating the region rich in colloid dimers, which provide intense plasmonic enhancement, we are able to achieve optimal SERS-based detection.

But using an aggregating agent does introduce a limitation. The channel accumulates Ag-NPs over time, some of which adhere on the channel walls. Accordingly, a given device was used for only approximately 10 min and only the data taken within that time frame are presented here.

RESULTS AND DISCUSSION

The detection scheme we use depends on the concerted action of mass transport, both advective and diffusive, with the aggregation reaction kinetics, as to create the desired degree of Ag-NP aggregation in areas of the channel where the analyte first diffuses. To achieve this, the Ag-NP aggregation reaction was studied in bulk solution prior to conducting microfluidic experiments. The reaction kinetics for the salt-induced Ag-NP aggregation was determined independently using UV−vis spectroscopy techniques as previously described.[25] The relative affinity constant for aggregate formation as a function of salt concentration, $k(c_s)/k_0$, was established, for the purposes of a numerical simulation, as a logarithmic sigmoid function with a sharp transition at around 100 mM LiCl, based on the UV−vis measurements. These measurements, and the corresponding sigmoidal function, are shown in Figure S1. The affinity function was used to numerically simulate the Ag-NP aggregation kinetics in the channel. Since only the relative aggregation constant, and not the absolute, was found by the UV−vis experiment, the magnitude of the maximum aggregation rate (k_0) is the only parameter that needs to be determined experimentally.

Numerical Simulation. The fluid flow and species transport in the device were calculated numerically for experimentally relevant conditions. For low-Reynolds number unidirectional flows ($Re = (\rho uL/\mu) \approx 10^{-2}$, where u and L are the relevant velocity and length scales), there is little mixing between the streams, and lateral mass transport occurs primarily through diffusion. The concentration profile of species i depends on its relative diffusivity D_i (we use the following naming scheme: i = A for the target analyte, i = S for salt, and i = 1, 2, 3, ..., for nanoparticle monomers, dimers, trimers, and so on for higher order aggregates), and can be adjusted by manipulating the flow Péclet number, $Pe_i = uL/D_i \approx 100$. The fastest diffusers in the system are the salt ions, which diffuse from the salt side-stream into the colloid side-stream, inducing aggregation of the Ag-NPs. We assume the NPs aggregate according to second-order reaction kinetics:

$$\begin{aligned} R_1 &= -2k(c_1c_1) - k(c_2c_1) - k(c_3c_1) \\ R_2 &= k(c_1c_1) - k(c_2c_1) - 2k(c_2c_2) \\ R_3 &= k(c_2c_1) - k(c_3c_1) \end{aligned} \quad (1)$$

where R_i is the rate of formation/depletion of species i, c_i its concentration, and the affinity, k, is a logarithmic sigmoid function of the salt concentration, as discussed above. The portion of the channel where the aggregation reaction is enabled by the presence of salt ions is shown in Figure S2. The computed steady state

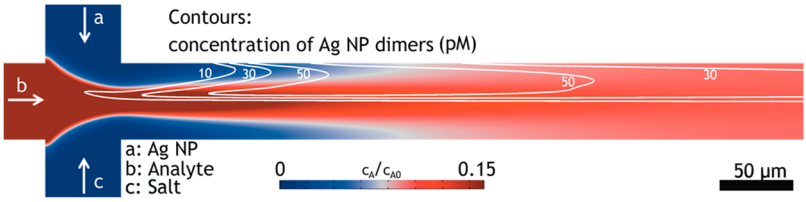

Figure 2. Numerical simulation of scalar transport in the device. Colormap: methamphetamine concentration (as a fraction of the initial concentration c_{A0}) in the flow-focusing device (truncated to a maximum of 15% of c_{A0} for clarity). Contours: concentration of silver nanoparticle dimers, exhibiting an area particularly rich in dimers immediately downstream from the junction.

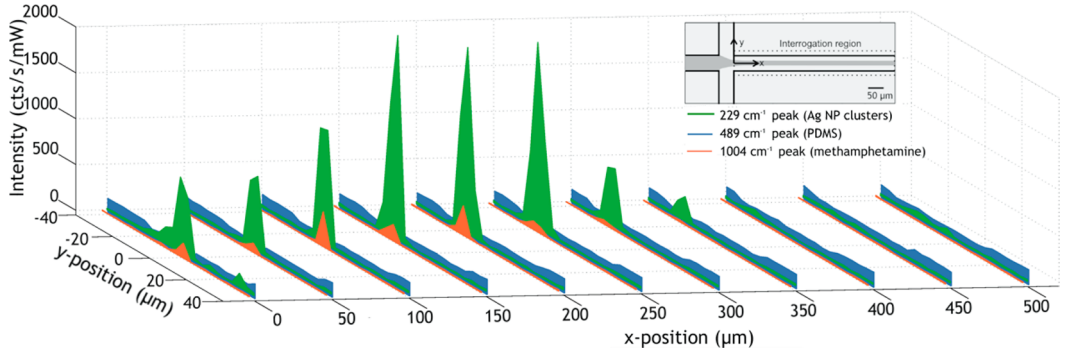

Figure 3. SERS intensities of selected Raman bands belonging to PDMS (blue), small Ag-NP aggregates (green), and methamphetamine (red). Overlaying the intensity of the peaks over the schematic of the channel (inset) produces a map that shows the aggregation profile of the nanoparticles, the diffusion profile of the analyte, and the channel walls.

concentration profiles for analyte and the nanoparticle dimers are shown in Figure 2. The calculation also yielded the steady state concentration of trimers and tetramers. The peak concentration of the trimers was ~40% of that of the dimer. Much lower concentrations were found for the tetramer. Aggregation starts at the junction, and the reaction proceeds while advecting to the right. This leads to the creation of an area of high concentration of nanoparticle dimers and trimers, which further downstream form larger aggregates that precipitate out of the flow and deposit on the walls of the channel. To capture the enhancement profile observed experimentally, the function was set to reach a maximum value $k_0 = 4 \times 10^{10}$ mol^{-1} s^{-1}.

SERS Measurements. Spectra were collected in an array of 11 by 21 points, spanning 500 μm along the channel and 80 μm across it, immediately downstream from the junction. The spectra demonstrated features strongly associated with their location in the channel, and the chemical species found there, thus providing a mapping of the species diffusion, and degree of NP aggregation in the channel. A characteristic collection of spectra acquired along a segment of a channel cross-section is shown in Figure S3. Most spectra contained the Raman signature of PDMS, with peaks at 489, 615, 708, 1261, and 1409 cm^{-1} as expected for areas with no plasmonic enhancement. In the region of the channel where aggregation was strongest, an intense peak at 229 cm^{-1} was observed, which has been previously convincingly attributed to an enhanced AgCl vibration.[30] This band has been used in several instances as a calibration band indicative of the degree of SERS enhancement.[31] In the regions of the Ag-NP stream that methamphetamine can reach by diffusion, spectra were observed which contain peaks at 1004, 1030, 1219, and 1600 cm^{-1}, all known methamphetamine Raman bands.[21,22,32,33]

By tracking the intensity of specific bands, the diffusion profile for methamphetamine can be determined, as well as the relative degree of Ag-NP aggregation as a function of location. The intensities of three selected peaks are plotted in Figure 3, as a function of their position in the channel for a sample with 10 nM of methamphetamine in saliva. The 489 cm^{-1} peak, corresponding to PDMS (blue), traces out the channel walls, while the 229 cm^{-1} peak intensity, associated with the presence of SERS-active Ag-NP clusters, is shown in green. Its profile was used to determine the k_0 parameter used in the simulation (Figure 2). The red line traces the 1004 cm^{-1} peak, associated with methamphetamine. Since this signal is dependent on the presence of Ag-NP aggregates, it largely tracks the green line.

This mapping represents a snapshot of the chemical processes in the channel after 1 min of flow and enables us to extract data during the initial stages of the aggregation reaction. Ag-NP dimers form readily after the junction through reactions of monomers. Under our flow and concentration conditions, higher order aggregates (which are formed through sequential addition of monomers to the dimer) are less abundant and their peak concentration locations occur

a little further downstream from the peak dimer position. At early times, dimers and, to a lesser extent, trimers dominate. This view is corroborated by the fact that the most intense SERS signals arise from the regions of the channel where our numerical simulations indicate the highest concentrations of dimers and trimers to be (Figures 2 and 3), with only the maximum aggregation parameter, k_0, fitted.

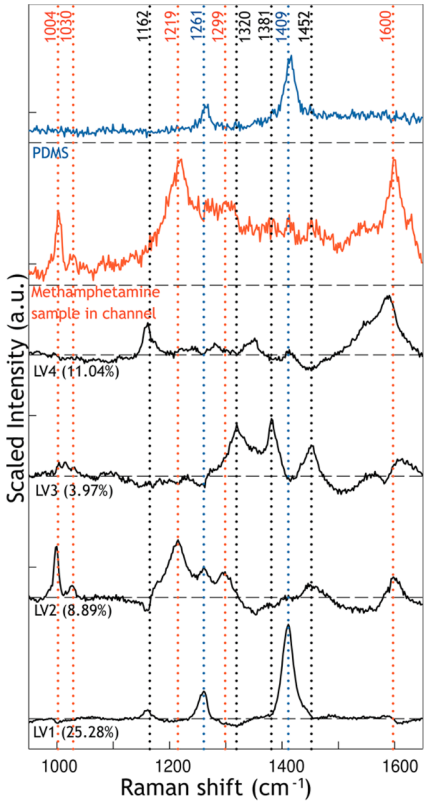

Figure 4. Latent Variables calculated for the calibration data after *varimax* rotation of the Principal Components. LV1 and LV2, respectively, capture variance of Raman Bands associated with PDMS and methamphetamine. LV3 was associated with features from citrate, and LV4 with broad fluorescent characteristics of SERS, and nonspecific peaks. Scaled experimental measurements of a PDMS control and a positive SERS measurement of methamphetamine from the device are also shown for comparison.

Data Analysis. Principal component analysis was employed to analyze the data. A model with four principal components (PCs) was created that captures the main systematic variance of the data, which stem from the chemical species involved. Subsequently, a *varimax* rotation was used as to decouple the obtained PCs into Latent Variables (LVs) (Figure 4). The LVs form a new set of basis vectors that span the same sample space as the original PCs. However, instead of aligning with the directions that maximize the variance captured, they now point to directions that describe the data with the simplest possible linear combinations of the LVs. Since the data used for the model are spectra of chemical species, this basis rotation allows us to obtain directions for our data that potentially correspond to chemically identifiable spectra.

LV1 captures the variance of the peaks associated with PDMS (1261 and 1409 cm^{-1}). LV2 appears to capture variance due the methamphetamine peaks (1004, 1030, 1219, 1299, and 1600 cm^{-1}) and was found a sufficient measure to separate the spectra exhibiting methamphetamine from the methamphetamine-negative spectra. LV3 presents features associated with the citrate spectrum (1320, 1381, and 1452 cm^{-1}) as citrate is the capping agent of the colloid used. Finally, LV4 is composed of broad features (around 1600 cm^{-1}), comprised primarily of the well-known enhanced SERS background,[34] as well as a band at 1165 cm^{-1}, possibly related to hydroxyl vibrations from the glass slide, and thus does not relate to the chemicals of interest.

This model was used to predict the presence of methamphetamine in the SERS spectra collected from the saliva samples. The scores on LV2 obtained from the saliva samples, shown in Figure 5, demonstrate

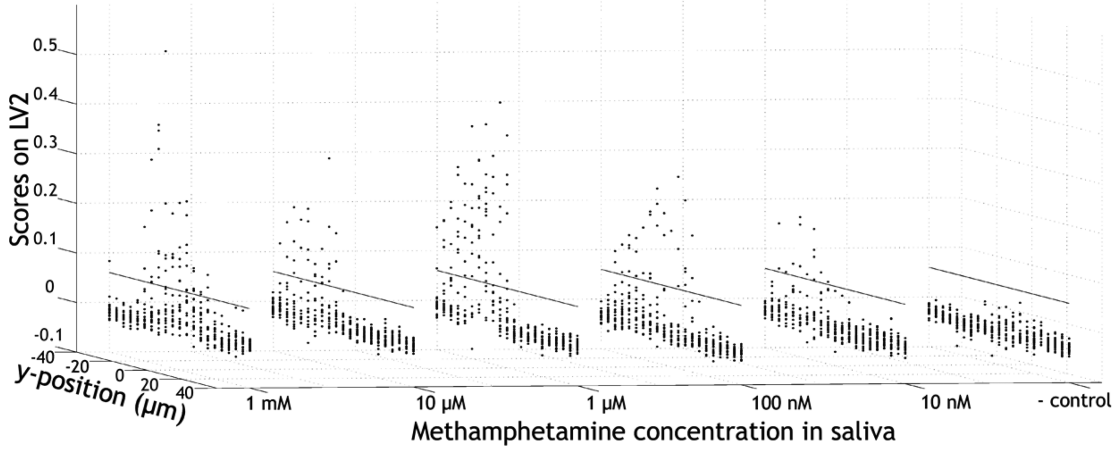

Figure 5. Predicted scores on LV2 of the experimental samples, based on the rotated PC model constructed from the calibration data, as a function of *y*-position (across the channel). The model correctly predicts methamphetamine-positive samples. An arbitrary threshold for detection was chosen as 0.06, and is denoted by a line for each condition. The *x*-position of the samples is not presented here; instead, all points collected in the streamwise direction are projected onto the *y*-axis.

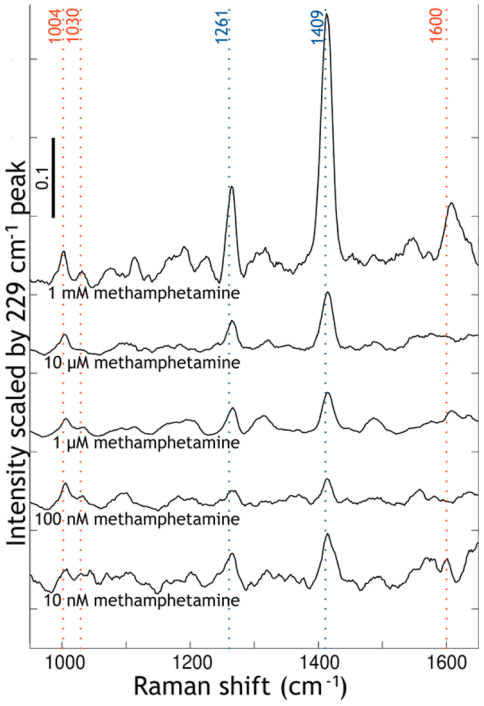

Figure 6. Average spectra of points with a score on LV2 greater than 0.06 from saliva samples. The spectra were normalized by the intensity of the 229 cm^{-1} peak (not shown), which dominates in cases were intense enhancement occurs. The characteristic peaks associated with methamphetamine at 1004 and 1030 cm^{-1} are present and of similar magnitude (approximately 0.05) for all concentrations after normalization, whereas the 1600 cm^{-1} peak is overtaken by broad fluorescence features for lower concentrations. The peaks attributed to PDMS (blue dotted lines) are ubiquitous.

that we are able to screen effectively for methamphetamine in the samples. As a negative control, a saliva sample with no added methamphetamine was used.

A score in LV2 greater than 0.06 was selected to count as a positive hit, but only if the sample exhibited low *q*-residuals (*q*-res < 0.15). The 95% confidence limit on LV2 for the model is 0.17, meaning that only 5% of the calibration data scored higher than this value. Spectra that fulfilled these criteria were averaged and plotted in Figure 6. The spectra were divided by the intensity of the 229 cm^{-1} peak, to normalize crudely for the number of aggregates contributing to the enhancement of each sample, and shifted on the *y*-axis for clarity. This normalization method scales the signal of the analyte with the degree of enhancement, greatly reducing the magnitude range of the relevant methamphetamine peaks. As a result, the previously constant PDMS bands now appear to fluctuate with methamphetamine concentration.

CONCLUSION

A microfluidic device was developed in which the transport and aggregation of SERS active silver nanoparticles could be explicitly controlled, and applied to the detection of methamphetamine in saliva. This microfluidic device exhibits several advantages over traditional SERS-based techniques: (i) The device facilitates the interaction of the nanoparticles and the analyte molecules in solution at the long interface along the parallel laminar flows. (ii) The controlled aggregation, induced by the salt solution, provides a reproducible and reliable region in which SERS signal is maximal. Interrogating this area makes the detection of broad classes of analytes possible with little dependence on the analyte's innate ability to induce aggregation. (iii) Finally, the size-dependent diffusivity of small molecules, such as methamphetamine, can be exploited to partially separate the analyte from other species present in a complex biological fluid, such as saliva.

Principal Components Analysis was shown to be an appropriate tool for the automated classification of the spectra. All experimental conditions, with the exception of the negative control, exhibited sufficiently high scores on LV2. The presence of methamphetamine in the sample was thus determined at concentrations as low as 10 nM, well below physiological quantities.

The results reported here provide evidence for a reproducible and rapid detection method that may be realized in the form of a cartridge-based microfluidic system that can be used to detect and identify narcotics in biological fluids within a few minutes. The device can potentially be used in other applications such as groundwater analysis and toxin detection.

MATERIALS AND METHODS

Microfluidic Device. The device was developed based on the design of Stiles *et al.*[35] such that the flow profile is solely determined by the device geometry. A single vacuum pump attached at the outlet was used to actuate the fluid flow. The channel dimensions were 20 μm deep by 50 μm wide, and the width of the focused stream was designed to be 5 μm. The mean flow velocity in the channel after the focusing junction was calculated to be 1.8 mm/s, and confirmed using micro particle-image velocimetry (μPIV).[36]

The microfluidic device was fabricated in PDMS (Sylgard 184) using standard soft lithography techniques and an SU-8 mold. Vias through the PDMS were made with a biopsy punch. Holes were drilled in a glass microscope slide and aligned with the vias. The PDMS was then sandwiched between a microscope coverslip (100 μm thick) and the drilled glass microscope slide, with the channel in direct contact with the coverslip as to provide unhindered optical access. Finally, pipet tips were inserted into the drilled holes to serve as fluid reservoirs.

Numerical Simulation. A numerical simulation of the fluid flow and the aggregation reaction was performed using COMSOL V4.3a (COMSOL, Stockholm, Sweden). The fluid motion in shallow microchannels can be simulated using the steady 2-D incompressible Navier–Stokes equations with the shallow

channel approximation.

$$\begin{aligned} \rho(\mathbf{u}\cdot\nabla)\mathbf{u} &= -\nabla p + \mu\nabla^2\mathbf{u} + \mathbf{F}_{HS} \\ \nabla\cdot\mathbf{u} &= 0 \end{aligned} \quad (2)$$

where $\mathbf{u}$ is the depth-averaged velocity, and ρ and μ are the fluid density and dynamic viscosity, respectively. The Hele-Shaw force term, $\mathbf{F}_{HS} = [-(12\mu/h^2)\mathbf{u}]$, accounts for the resistance to flow due to the out-of-plane walls in the shallow channel approximation. The steady concentration fields follow the steady state scalar advection equation

$$(\mathbf{u}\cdot\nabla)c_i = \nabla\cdot(D_i\nabla c_i) + R_i \quad (3)$$

where c_i is the concentration of species *i*. using the same naming scheme as in eq 1. The diffusivity for each species is estimated using the Stokes−Einstein equation, $D_i = k_BT/6\pi\mu r_i$ where k_BT is the thermal energy and r_i is the Stokes radius of the species *i*.

The simulation geometry is based on the design of the microfluidic flow-focusing device used in the experiments, shown schematically in Figure 1. The fluid and concentration fields were estimated by numerically simulating eqs 1−3 with the appropriate boundary conditions.

We estimated the diffusivity constants as follows: $D_A = 1.00 \times 10^{-9}$ m^2/s for methamphetamine, $D_S = 1.96 \times 10^{-9}$ m^2/s for the salt ions, and $D_i = 1.00 \times 10^{-11}$ m^2/s for the colloid monomers and higher order aggregates. The aggregation affinity was approximated by a logarithmic sigmoidal function reaching 0.5 at 100 mM of LiCl, with 0.1−0.9 rise over an interval of 200 mM, shown in Figure S1.

Saliva Sample Preparation. Saliva was collected from a healthy, drug-free, volunteer, at least 1 h after a meal, diluted with equal volume of DI water, and aliquots of the mixture were spiked with (+)-methamphetamine hydrochloride (Sigma-Aldrich) to prepare sample concentrations of 0 nM, 10 nM, 100 nM, 1 μM, 10 μM, and 1 mM of the chemical. The saliva/DI samples were filtered using 0.45 μm Nalgene filters immediately prior to loading into the device, to prevent blocking of the microchannel by particulates. A separate solution of 1 mM methamphetamine in DI water was used to acquire a positive identification of the SERS signature as a reference. A negative control in DI was also used in the experiment.

Reagents. The silver colloid used was citrate-capped BioPure 20 nm silver (nanoComposix, Inc., San Diego, CA) diluted to 1:100 from stock solution with DI water. A 1 M aqueous LiCl solution was used as the aggregation-inducing agent.

Experimental Procedure. Approximately 20 μL each of sample, colloid, and salt solution were loaded into the device reservoirs using syringes. A new microfluidic device was used for each experiment to avoid cross-contamination. For each run, the device was placed onto the spectrometer microscope stage, centered, and aligned. The vacuum pump was connected to the outlet of the device with PTFE tubing. The device was allowed to run for 1 min prior to the collection of spectra, to ensure steady flow. Spectra, excited by 3.8 mW of 633 nm laser light, were collected using a LabRam Aramis spectrometer (Horiba, Kyoto, JP) in an array of 11 by 21 points, spanning 500 μm along the channel and 80 μm across it. The diameter of the interrogation spot was focused to a diameter 2 μm, and each point was interrogated for 0.5 s.

Data Analysis. Principal component analysis (PCA) was performed on the data using the PLS Toolbox (Eigenvector Research, Inc.., Wenatchee, WA) to categorize the spectra. A statistical model was constructed using the spectra from the calibration experiments (1 mM methamphetamine in DI) and a negative control (only DI). The spectra were preprocessed by sequential application of baseline subtraction using a weighted least-squares method, normalization by the areas under the spectrum between 1049 and 1152 and 1468−1538 cm^{-1}, and finally mean-centering. Only spectral features between 900 and 1650 cm^{-1} were included in the regression analysis.

Conflict of Interest: The authors declare no competing financial interest.

Acknowledgment. The authors thank K. Plaxco and members of his laboratory for their contributions in materials and discussions, as well as B. Piorek for his guidance regarding the statistical analysis. The fabrication was undertaken in the University of California, Santa Barbara, Nanofabrication Facility, part of the National Science Foundation-funded National Nanofabrication Infrastructure Network. The bulk nanoparticle aggregation rates were measured in the Biological Nanostructures Laboratory. This work is supported in part by the Institute for Collaborative Biotechnologies through contract no. W911NF-09-D-0001 from the U.S. Army Research Office The content of the information does not necessarily reflect the position or the policy of the Government, and no official endorsement should be inferred.

Supporting Information Available: Additional experimental details and figures. This material is available free of charge *via* the Internet at http://pubs.acs.org.

REFERENCES AND NOTES

1. UNODC. *World Drug Report 2012*, United Nations publication, Sales No. E.12.XI.1; United Nations: New York, **2012**.
2. Cone, E. J. Saliva Testing for Drugs of Abuse. *Ann. N.Y. Acad. Sci.* **1993**, *694*, 91–127.
3. Schepers, R. J.; Oyler, J. M.; Joseph, R. E.; Cone, E. J.; Moolchan, E. T.; Huestis, M. A. Methamphetamine and Amphetamine Pharmacokinetics in Oral Fluid and Plasma after Controlled Oral Methamphetamine Administration to Human Volunteers. *Clin. Chem.* **2003**, *49*, 121–132.
4. Huestis, M. A.; Cone, E. J. Methamphetamine Disposition in Oral Fluid, Plasma, and Urine. *Ann. N.Y. Acad. Sci.* **2007**, *1098*, 104–121.
5. Han, E.; Miller, E.; Lee, J.; Park, Y.; Lim, M.; Chung, H.; Wylie, F. M.; Oliver, J. S. Validation of the Immunalysis® Microplate ELISA for the Detection of Methamphetamine in Hair. *J. Anal. Toxicol.* **2006**, *30*, 380–385.
6. Pujol, M. L.; Cirimele, V.; Tritsch, P. J.; Villain, M.; Kintz, P. Evaluation of the IDS One-Step ELISA Kits for the Detection of Illicit Drugs in Hair. *Forensic Sci. Int.* **2007**, *170*, 189–192.
7. Strano-Rossi, S.; Colamonici, C.; Botrè, F. Parallel Analysis of Stimulants in Saliva and Urine by Gas Chromatography/Mass Spectrometry: Perspectives for "in Competition" Anti-Doping Analysis. *Anal. Chim. Acta* **2008**, *606*, 217–222.
8. Al-Dirbashi, O. Y.; Kuroda, N.; Wada, M.; Takahashi, M.; Nakashima, K. Quantification of Methamphetamine, Amphetamine and Enantiomers by Semi-micro Column HPLC with Fluorescence Detection; Applications on Abusers' Single Hair Analyses. *Biomed. Chromatogr.* **2000**, *14*, 293–300.
9. Nakashima, K.; Suetsugu, K.; Yoshida, K.; Akiyama, S.; Uzu, S.; Imai, K. High Performance Liquid Chromatography with Chemiluminescence Detection of Methamphetamine and its Related Compounds using 4-(N, N-dimethylaminosulphonyl)-7-fluoro-2, 1, 3-benzoxadiazole. *Biomed. Chromatogr.* **2005**, *6*, 149–154.
10. Khan, J. I.; Kennedy, T. J.; Christian, D. R. Chemical Screening. In *Basic Principles of Forensic Chemistry*; Humana Press: New York, 2012; pp 79−90.
11. Mogensen, K. B.; Klank, H.; Kutter, J. P. Recent Developments in Detection for Microfluidic Systems. *Electrophoresis* **2004**, *25*, 3498–3512.
12. Vandaveer, W. R.; Pasas-Farmer, S. A.; Fischer, D. J.; Frankenfeld, C. N.; Lunte, S. M. Recent Developments in Electrochemical Detection for Microchip Capillary Electrophoresis. *Electrophoresis* **2004**, *25*, 3528–3549.
13. Lim, C.; Hong, J.; Chung, B. G.; Choo, J. Optofluidic Platforms Based on Surface-Enhanced Raman Scattering. *Analyst* **2010**, *135*, 837–844.
14. Jeanmaire, D. L.; Van Duyne, R. P. Surface Raman Spectroelectrochemistry: Part I. Heterocyclic, Aromatic, and Aliphatic Amines Adsorbed on the Anodized Silver Electrode. *J. Electroanal. Chem. Interfacial Electrochem.* **1977**, *84*, 1–20.
15. Michaels, A.; Nirmal, M.; Brus, L. E. Surface Enhanced Raman Spectroscopy of Individual Rhodamine 6G Molecules on Large Ag Nanocrystals. *J. Am. Chem. Soc.* **1999**, *121*, 9932–9939.

16. Le Ru, E. C.; Meyer, M.; Etchegoin, P. G. Proof of Single-Molecule Sensitivity in Surface Enhanced Raman Scattering (SERS) by Means of a Two-Analyte Technique. *J. Phys. Chem. B* **2006**, *110*, 1944–1948.
17. Inscore, F.; Shende, C.; Sengupta, A.; Huang, H.; Farquharson, S. Detection of Drugs of Abuse in Saliva by Surface-Enhanced Raman Spectroscopy (SERS). *Appl. Spectrosc.* **2011**, *65*, 1004–1008.
18. Piorek, B. D.; Lee, S. J.; Santiago, J. G.; Moskovits, M.; Banerjee, S.; Meinhart, C. D. Free-Surface Microfluidic Control of Surface-Enhanced Raman Spectroscopy for the Optimized Detection of Airborne Molecules. *Proc. Natl. Acad. Sci. U.S.A.* **2007**, *104*, 18898–18901.
19. Piorek, B. D.; Lee, S. J.; Moskovits, M.; Meinhart, C. D. Free-Surface Microfluidics/SERS for Real-Time Trace Vapor Detection of Explosives. *Anal. Chem.* **2012**, *84*, 9700–9705.
20. Hering, K.; Cialla, D.; Ackermann, K.; Dörfer, T.; Möller, R.; Schneidewind, H.; Mattheis, R.; Fritzsche, W.; Rosch, P.; Popp, J. SERS: A Versatile Tool in Chemical and Biochemical Diagnostics. *Anal. Bioanal. Chem.* **2008**, *390*, 113–124.
21. Sulk, R. A.; Corcoran, R. C.; Carron, K. T. Surface-Enhanced Raman Scattering Detection of Amphetamine and Methamphetamine by Modification with 2-Mercaptonicotinic Acid. *Appl. Spectrosc.* **1999**, *53*, 954–959.
22. Anyu, C.; Lin, H.; Jinghua, L.; ZiJian, C.; Yi, J.; Dian, Q.; Xun, G.; Chunwei, L.; Wen, H.; Hong, W. Detecting Narcotic Usage Using Surface-Enhanced Raman Spectroscopy on Saliva Samples. In *World Congress on Medical Physics and Biomedical Engineering, September 7−12, 2009, Munich, Germany*; Springer: Berlin, Heidelberg, 2009; pp 71−74.
23. Moskovits, M.; Tay, L. L.; Yang, J.; Haslett, T. SERS and the Single Molecule. In *Optical Properties of Nanostructured Random Media*; Springer: Berlin, Heidelberg, 2002; pp 215−227.
24. Derjaguin, B. V.; Landau, L. The Theory of Stability of Highly Charged Lyophobic Sols and Coalescence of Highly Charged Particles in Electrolyte Solutions. *Acta Physicochim. URSS* **1941**, *14*, 633–652.
25. Moskovits, M.; Vlčková, B. Adsorbate-Induced Silver Nanoparticle Aggregation Kinetics. *J. Phys. Chem. B* **2005**, *109*, 14755–14758.
26. Martin, J. E.; Wilcoxon, J. P.; Schaefer, D.; Odinek, J. Fast Aggregation of Colloidal Silica. *Phys. Rev. A* **1990**, *41*, 4379.
27. Löwen, H.; Madden, P. A.; Hansen, J. P. Ab initio Description of Counterion Screening in Colloidal Suspensions. *Phys. Rev. Lett.* **1992**, *68*, 1081–1084.
28. Traube, J.; Rackwitz, E. Ueber die Wirkung von Schutzkolloiden. *Colloid Polym. Sci.* **1925**, *37*, 131–138.
29. Langmuir, I. The Constitution and Fundamental Properties of Solids and Liquids. II. Liquids. *J. Am. Chem. Soc.* **1917**, *39*, 1848–1906.
30. Guerrini, L.; Garcia-Ramos, J. V.; Domingo, C.; Sanchez-Cortes, S. Nanosensors Based on Viologen Functionalized Silver Nanoparticles: Few Molecules Surface-Enhanced Raman Spectroscopy Detection of Polycyclic Aromatic Hydrocarbons in Interparticle Hot Spots. *Anal. Chem.* **2009**, *81*, 1418–1425.
31. Caro, C.; Lopez-Cartes, C.; Zaderenko, P.; Mejias, J. A. Thiol-Immobilized Silver Nanoparticle Aggregate Films for Surface Enhanced Raman Scattering. *J. Raman Spectrosc.* **2008**, *39*, 1162–1169.
32. Angel, S. M.; Roe, J. N.; Andresen, B. D.; Myrick, M. L.; Milanovich, F. P. Development of a Drug Assay Using Surface-Enhanced Raman Spectroscopy. *Proc. SPIE 1201* **1990**, 469–473.
33. Sägmüller, B.; Schwarze, B.; Brehm, G.; Trachta, G.; Schneider, S. Identification of Illicit Drugs by a Combination of Liquid Chromatography and Surface-Enhanced Raman Scattering Spectroscopy. *J. Mol. Struct.* **2003**, *661*, 279–290.
34. Mahajan, S.; Cole, R. M.; Speed, J. D.; Pelfrey, S. H.; Russell, A. E.; Bartlett, P. N.; Barnett, S. M.; Baumberg, J. J. Understanding the Surface-Enhanced Raman Spectroscopy "Background. *J. Phys. Chem. C* **2010**, *114*, 7242–7250.
35. Stiles, T.; Fallon, R.; Vestad, T.; Oakey, J.; Marr, D. W. M.; Squier, J.; Jimenez, R. Hydrodynamic Focusing for Vacuum-Pumped Microfluidics. *Microfluid. Nanofluid.* **2005**, *1*, 280–283.
36. Meinhart, C. D.; Wereley, S. T.; Santiago, J. G. PIV Measurements of a Microchannel Flow. *Exp. Fluids* **1999**, *27*, 414–419.